Band structures and optical spectra of InN polymorphs: Influence of quasiparticle and excitonic effects

J. Furthmüller, P. H. Hahn, F. Fuchs, and F. Bechstedt
Institut für Festkörpertheorie und -optik, Friedrich-Schiller-Universität, Max-Wien-Platz 1, 07743 Jena, Germany
(Received 3 June 2005; published 3 November 2005)

We present *ab initio* calculations of the electronic structure and the optical properties of InN crystallizing in wurtzite, zinc-blende, and rocksalt structures. They are based on well converged atomic geometries including the effect of the In 4*d* electrons. The quasiparticle aspect is described in the framework of a *GW* approximation. The opposite influence of quasiparticle effects and the *pd* repulsion is demonstrated for the band structures. The pecularities of the band structures such as the small gap of the 2*H* and 3*C* polymorphs and their large electron affinity are discussed. The frequency dependence of the dielectric functions is explained in terms of nonparabolic bands and high-energy optical transitions at critical points. Excitonic effects drastically influence the optical absorption by an overall redshift of the entire spectrum and a redistribution of oscillator strengths. The results are critically discussed in the light of recent experiments.

DOI: 10.1103/PhysRevB.72.205106 PACS number(s): 71.20.Nr, 78.20.Bh, 71.15.Mb

I. INTRODUCTION

Recently, InN has attracted considerable attention due to its potential applications, on one side, and the seemingly conflicting results of various investigations, on the other side. Most important were the repeated observations of an effective band gap of about 0.7 eV by optical techniques,[1–3] in contrast to the value of 1.9 eV[4] established for the last 20 years. Only isolated groups (see, e.g., Ref. 5) claim to observe a gap of InN in between the mentioned values. However, more recent measurements,[6–8] which[7] have been partly performed also by authors of Ref. 5, have again proven the small gap value of InN. The smaller band gap value extends the possible emission range of optoelectronic devices based on group-III nitrides from deep-uv (AlN) down to the near-ir region (InN). Further potential applications of InN are suggested because of its superior transport properties.[9] The material apparently has the smallest effective electron mass among the nitrides but perhaps also of all semiconductors. Predictions of a large saturation velocity and an extremely high drift velocity (at room temperature) make InN a promising material for high-speed and high-frequency electronic devices.

The growth of InN is very difficult due to the low dissociation temperature and the extremely high equilibrium vapor pressure of nitrogen. Nevertheless, in the last four years, considerable progress has been made to grow epitaxial hexagonal InN films by molecular beam epitaxy (MBE)[1,2] and metalorganic vapor phase epitaxy[3] (MOVPE). Though the hexagonal wurtzite (*w*, 2*H*) phase with space group $P6_3mc$ (C_{6v}^4) is the thermodynamically stable one under ordinary conditions,[10,11] also, successful growth[12,13] by MBE has been reported for cubic InN crystallizing in zinc-blende (*zb*, 3*C*) structure with space group $F\bar{4}3m$ (T_d^2). Theoretical studies based on total-energy calculations[14,15] clearly predict a first-order phase transformation from the wurtzite into the rocksalt (*rs*, NaCl) structure with space group $Fm3m$ (O_h^5) under hydrostatic pressure. This is confirmed experimentally with a transition pressure of about 12.1 GPa.[16]

Theoretical studies[14,15,17–22] of the atomic structures, in particular the lattice constants, are usually based on the density functional theory[23] (DFT). They give a unique picture if the In 4*d* electrons are included in the calculations.[17] Deviations arise mainly from the treatment of exchange and correlation (XC) within the local density approximation[24] (LDA) or the generalized gradient approximation[25,26] (GGA), as can be seen by comparison of results from Refs. 18 and 20. Other small deviations are due to the treatment of the electron-ion interaction and the expansion of wave functions in a certain basis set. Much more confusing are the results of various theoretical studies. It is well known that the density functional theory in LDA or GGA, which is widely used in modern band-structure calculations, severely underestimates the fundamental gaps and transition energies of semiconductors and insulators.[27,28] For example, the band gaps of GaN (2.3 eV) and AlN (3.9 eV)[29] are much smaller than the quasiparticle values of about 3.5 and 5.8 eV, respectively, which are close to the experimental gap energies. For InN the DFT-LDA and DFT-GGA calculations usually give rise to negative energy gaps between 0.0 and −0.3 eV for wurtzite and somewhat more negative values for zinc blende if the In 4*d* electrons are taken into account.[14,18–21,30,31] Similar results are obtained using the relativistic full-potential Korringa-Kohn-Rostocker method.[32] Only methods which allow manipulations of the electron-ion interaction or the exchange-correlation potential report positive gaps. For instance, using self-interaction and relaxation corrected pseudopotentials, Vogel *et al.*[31,33] find gaps of 1.3 eV (3*C*) and 1.6 eV (2*H*). A similar method[20] with In 4*d* electrons frozen into the core gives smaller values of 0.43 eV (3*C*) and 0.58 eV (2*H*). Changing the XC potential[34] and taking into account the screened exchange[35] or the exact exchange[36] open the gaps. For InN, the gap opening due to quasiparticle corrections depends on the details of the *GW* approximation used.[20,21,30,34,37] Using certain semiempirical LDA-based methods,[37] gaps of the correct magnitude, 0.70 eV (3*C*) and 0.85 eV (2*H*) may be obtained. However, why a certain implementation of the linear combination of atomic orbitals

(LCAO) method in the DFT-LDA (Ref. 22), i.e., a theory which does not take the excitation aspect into account, should give correct gaps of 0.88 eV (2*H*) and 0.65 eV (3*C*), remains an open question to the authors. Of course, calculations within the empirical pseudopotential theory[38,39] give gap values in agreement with the used input fit parameters, but cannot predict gaps as sometimes written in certain (also theoretical) publications. Despite so many theoretical results indicating a fundamental gap of wurtzite InN below 1 eV, as well as such low values from absorption measurements,[1–3,6–8] there are still doubts claiming larger gap values (cf. discussion in Ref. 40).

So far, optical properties or, more precisely, the frequency-dependent dielectric function have been calculated for 2*H* and 3*C* InN[14,20,21,34] only within the independent-particle or independent-quasiparticle approach.[41] The imaginary part shows a characteristic line shape. There is a steep onset of the absorption which changes over into a rather constant part. The transition region is either characterized by a kink or even a small peak. The high-energy region between 5 and 15 eV shows a variety of strong peaks that are sometimes related to critical points and interband transitions in the band structure. In principle, such a frequency variation has also been measured using spectroscopic ellipsometry.[6–8,42] The real part of the dielectric function shows a corresponding behavior. However, there occurs a low-energy peak at about 1 eV. For very low frequencies, an electronic high-frequency dielectric constant of about 7–8 is found. The anisotropy splitting in the wurtzite case is of the order of magnitude of 0.3.

In this paper, we present a careful study of the quasiparticle band structures of the InN polymorphs crystallizing in wurtzite, zinc-blende, and rocksalt structures. They are based on high-precision total-energy optimizations of their atomic structures including the In 4*d* electrons. The effect of the *d* electrons on the band energies is discussed in detail. The region of the fundamental gap around Γ as well as the energy bands at other high-symmetry points in the Brillouin zone (BZ) are given. Based on the electronic structure results in quasiparticle approximation, both the real and imaginary part of the dielectric function are computed. In a last step also excitonic effects such as the attractive screened Coulomb interaction of electrons and holes as well as the electron-hole exchange are taken into account. A detailed comparison with experimental spectra is planned.

II. COMPUTATIONAL METHODS

A. Ground-state properties

The calculations are based on the DFT (Ref. 23) in the LDA (Ref. 24). The Perdew-Zunger interpolation formula[43] is applied to describe the electron density dependence of the XC energy. We use a plane-wave expansion of the eigenfunctions and nonnormconserving pseudopotentials as implemented in the Vienna *ab initio* simulation package[44] (VASP). The In 4*d* electrons are treated as valence electrons. This approximation called "*d*val" guarantees correct structural properties of the InN polymorphs.[17] The use of ultrasoft pseudopotentials allows a remarkable reduction of the plane-wave cutoff to 16.2 Ry. The eigenvalues of the Kohn-Sham equation[24] give a first approach to reliable band structures of the InN polymorphs. For the purpose of comparison, we also use another type of pseudopotentials which account for self-interaction corrections (SICs) of the 4*d* electrons in the underlying free-atom calculation but freeze the In 4*d* electrons into the core in the solid-state calculations.[45] The atomic positions are kept fixed in the positions obtained within the *d*val approach. The comparison of the band structures computed within the *d*val and SIC approximations indicates the influence of the shallow In 4*d* levels on the valence states.

B. Quasiparticle and optical properties

The use of nonnormconserving pseudopotentials does not automatically give a set of orthonormalized wave functions. For that reason, we combine the electronic-structure calculations within the SIC approach with the projector-augmented wave (PAW) method.[46,47] Using projectors onto the core regions of the free atoms and pseudoatoms, all-electron wave functions are constructed for the valence electrons. They allow us the computation of the XC self-energy in *GW* approximation[48,49] and the optical transition operator.[47] Since the SIC approximation gives the correct energetical ordering and occupation of the bands, the quasiparticle effect is treated in the standard manner[27,28] within first-order perturbation theory. No update of the quasiparticle wave functions with respect to the solutions of the Kohn-Sham equation[24] is taken into account. In a first step, complete optical spectra are calculated in the independent-particle (starting from the SIC electronic structure) or independent-quasiparticle approach.[41] Together with the local electron densities, the dielectric constants obtained within the independent-quasiparticle approach are used to model the screening properties of the InN systems.[48,49]

C. Coulomb-correlated electron-hole pairs

In the case of the optical properties and, hence, the calculation of the frequency-dependent dielectric functions, the description of the excited particles, electrons and holes, as quasiparticles is not sufficient. There are additional many-body effects related to the mutual interaction of the excited electrons and holes, for instance, the direct Coulomb attraction of these particles and the electron-hole exchange.[50]

The corresponding Bethe-Salpeter equation (BSE) for the macroscopic polarization function can be solved using different methods.[51–53] Within the standard approach,[51,53] the eigenvalues and eigenvectors of the corresponding two-particle Hamiltonian are used to calculate the polarization function and, consequently, the frequency-dependent dielectric function including quasiparticle and excitonic effects. In the wurtzite case, the Hamiltonian has been set up from eight valence bands and eight conduction bands at 4704 Monkhorst-Pack (MP) **k** points[54] in the full BZ. In order to bypass the diagonalization of the Hamiltonian, we follow a new formulation for the time-dependent optical polarization.[55] Its time evolution is driven by the two-particle Hamiltonian, and its initial value is defined by the optical transition matrix elements. The Fourier transformation with a

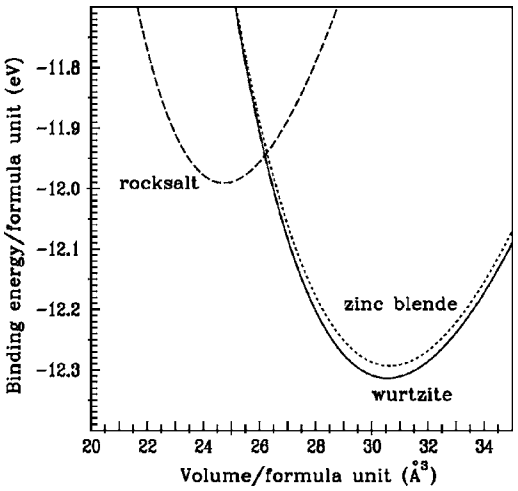

FIG. 1. The normalized total energy versus volume for one In—N pair. Three different polymorphs have been studied: wurtzite (solid line), zinc blende (dotted line), and rocksalt (dashed line).

certain broadening parameter γ leads to the frequency-dependent optical polarization. It has been demonstrated[55] that this method is particularly efficient for systems with many pair states, such as surfaces[56] and solids with large unit cells.[57]

III. ATOMIC GEOMETRIES AND ENERGETICS

The minimization of the total energies of the three polymorphs wurtzite (*w*), zinc blende (*zb*), and rocksalt (*rs*) has been performed replacing Brillouin-zone summations by special points according to Monkhorst and Pack.[54] In the case of the fcc Bravais lattice, an equidistant $8\times8\times8$ mesh has been used; whereas in the case of the hexagonal Bravais lattice, we applied a $25\times25\times16$ mesh. The slightly higher density of mesh points is a consequence of the higher accuracy requirements to determine the three independent lattice parameters a, c, and u in the wurtzite case in comparison to the cubic polymorphs which are characterized only by a lattice constant a_0. The resulting energy-volume dependences have been obtained from a fit to the Murnaghan equation of state.[58] They are represented in Fig. 1. The fit leads to the equilibrium parameters for the volume Ω_0 (and, hence, one lattice constant), the binding energy E_B per atom pair, the bulk modulus B, and its pressure coefficient $B'=(dB/dp)_{p=0}$. These parameters are summarized together with the lattice parameters in Table I.

The energetical ordering of the three phases considered in Fig. 1 and Table I is in agreement with other calculations. This holds in particular for the energy gain of about 20 meV per cation-anion pair of the wurtzite structure versus the zinc-blende polytype.[18,19,59] However, also the reduction of the pair volume to 80.9% and the transition pressure of about 9.0 GPa for the pressure-induced wurtzite-rocksalt phase transition are in agreement with other calculations.[14,15] The calculated transition pressure is somewhat smaller than the experimental one of about 12.1 GPa, while the volume reduction of 19.1% is very close to the 17.6% found experimentally.[16] The isothermal bulk modulus B and its pressure derivative B' in Table I come close to values published in the literature for the InN polymorphs.[14,17–19,22] The experimental value of 1.26 Mbar measured for a low-quality wurtzite crystal[16] is somewhat smaller.

The calculated lattice parameters in Table I are in excellent agreement with other pseudopotential calculations using the LDA framework[17,18] but are smaller compared with GGA results.[19] In particular, there is excellent agreement of the calculations with the measured value of the parameter $u=0.3769$.[60] Taking into account the tendency for underestimation of the lattice parameters within the LDA, the agreement with measured values is excellent. Juza and Hahn[61] first reported the crystalline structure of InN to be wurtzite having lattice parameters $a=3.53$ Å and $c=5.69$ Å. The lattice parameters measured recently in high-quality hexagonal InN films were found to be $a=3.5365$ Å and $c=5.7039$ Å.[1] The deviations of the theoretical values are below 0.4%. All these results show that the critical parameters $\Delta(c/a)=c/a-(c/a)_{\text{ideal}}$ and $\Delta u=u-u_{\text{ideal}}$ with the ideal values $c/a=\sqrt{8/3}$ and $u=3/8$ are small. The negative value $\Delta(c/a)=-0.018$ is clearly correlated with the fact that the wurtzite structure corresponds to the equilibrium polymorph.[10,11] The deviations from experimental values are similar in the zinc-blende case. X-ray diffraction (XRD) measurements gave a value of $a_0=4.98$ Å. Data for the high-pressure rocksalt phase indicate a 17.6% reduction of the relative volume with respect to the wurtzite case.[16] This results in a lattice constant of about $a_0=4.67$ Å. The 1% discrepancy may be, however, a consequence of the used low-quality InN sample containing or contaminated by indium oxides.

IV. BAND STRUCTURES

A. Influence of the *pd* repulsion

For the equilibrium lattice parameters the Kohn-Sham (KS) equation on the DFT-LDA (Ref. 24) can also be solved at **k** points of high-symmetry lines in the BZ of the considered InN polymorph. The eigenvalues versus these **k** points give the Kohn-Sham band structures. We will not present such band structures because of three facts. (i) The In 4*d*

TABLE I. Structural and energetical parameters of three InN polymorphs.

Polymorph	Ω_0 (Å^3)	E_B (eV)	B (Mbar)	B'	Lattice Parameter
wurtzite	30.56	12.314	1.413	4.48	$a=3.5226$ Å, $c=5.6880$ Å, $u=0.3789$
zinc blende	30.64	12.293	1.415	3.75	$a_0=4.9670$ Å
rocksalt	24.72	11.991	1.870	4.92	$a_0=4.6245$ Å

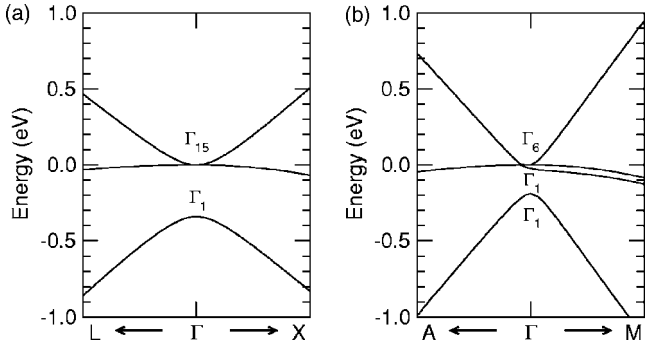

FIG. 2. The band structures of *zb*-InN (a) and *w*-InN (b) around the Fermi level (used as energy zero) close to the Γ point. They are computed within DFT-LDA and treating the In 4*d* electrons as valence electrons.

levels appear in the lowest, almost N 2*s*-like valence bands.[62] The hybridization of In 4*d* and N 2*s* states gives rise to certain splittings. In reality, the In 4*d* peaks are usually found below the lowest *s*-like bands in a distance of about 14.9 eV[63] or 16.7 eV[64] (or even 16.9 eV[65]) to the valence band maximum (VBM). (ii) The KS gap of *rs*-InN is opened to 1.07 eV due to the reduction of the volume per cation-anion pair. However, as also observed by other DFT-LDA calculations treating the In 4*d* electrons as valence electrons,[17–20] we find a negative *sp* gap, i.e., a negative distance of the $\Gamma_{1c}-\Gamma_{15v}$ (zinc blende) and $\Gamma_{1c}-\Gamma_{6v}/\Gamma_{1v}$ (wurtzite) levels. (iii) In the wurtzite case, the crystal-field splitting $\Delta_{cr}=\varepsilon(\Gamma_{6v})-\varepsilon(\Gamma_{1v})$[62] amounts to a positive value $\Delta_{cr}=15.4$ meV.

The wrong energetical ordering of the *s*-state and *p*-states near the Fermi level for 3*C*-InN and 2*H*-InN does not really give rise to "systems with negative gap" or "metallic systems" as is sometimes written in the literature. Rather, zero-gap semiconductors are calculated. In the zinc-blende case, an "inverted band structure" occurs near the Γ point which is typical for the zero-gap semiconductors such as HgTe (which, however, is remarkably modified by the spin-orbit interaction).[66] For vanishing spin-orbit coupling, this situation is illustrated in Fig. 2. The situation is similar for the wurtzite structure, only the Γ_{15v} level is split into Γ_{6v} and Γ_{1v} due to the crystal field.

The reason of the "negative gaps" $\Gamma_{1c}-\Gamma_{15v}$ and $\Gamma_{1c}-\Gamma_{6v}$ is of course a consequence of the studied KS band structure being characteristic for the ground state of the systems. Measurements of the band structure by means of photoemission/inverse photoemission or optical methods are always related to single-particle or two-particle electronic excitations. The corresponding quasiparticle effects are responsible for the increase of all gaps and transition energies between occupied and empty bands. They can be treated within perturbation theory.[27,28] Such a gap opening of about 0.8 eV[18] happens for *rs*-InN using the Bechstedt-Del Sole formula.[67] However, the first-order perturbation theory cannot be applied in the case of *zb*-InN and *w*-InN because of the wrong energetical ordering of the bands near the "band gap" and the hybridization of the "lowest valence bands" with the shallow In 4*d* core levels. The electronic structures of these systems need a self-consistent procedure with an update of the quasiparticle wave functions.[30,68]

The self-consistent procedure, which is extremely computer time consuming, can be avoided by understanding the physics of the appearing "wrong" band orderings. Within LDA, the energetical distance of the Γ_{15v} or Γ_{6v}/Γ_{1v} VBM to the In 4*d* bands is with about 13.5 eV remarkably underestimated with respect to the experimental values. As a consequence, the *pd* repulsion[69] of the mainly *p*-like VBM and the shallow core levels is overestimated. This results in a too strong pushing of the VBM toward higher energies and, hence, a negative gap. The tendency of the negative gap is enforced by the low-lying *s*-like Γ_{1c} "conduction band." The material InN, at least in its 2*H* or 3*C* polytypes, has extremely large electron affinities due to the much weaker overlap of *s* orbitals localized at nearest-neighbor atoms.[18,70] Colleagues argue[37] that the tendency for a small InN gap (e.g., in comparison with InP) is due to the combined effects of the much lower N 2*s* orbital energy and the much smaller band-gap deformation potential for the more ionic InN. The large gap of *rs*-InN indicates that these arguments are not completely true. Only the argument with the deformation potential goes in the same direction of the small nearest-neighbor interaction. It is, however, obvious that an essential hybridization of In 4*d* states and anion *s* states can only happen in InN but not in InP.

In order to make more clear the crucial effect of the In 4*d* states on the important bands, we have also performed calculations where the In 4*d* electrons are frozen into the core in the solid-state calculations. The effect of these electrons, however, is considered in constructing the pseudopotentials. Self-interaction corrections are taken into account in the underlying atomic calculations.[45] The electronic-structure calculations within the Kohn-Sham framework at the theoretical lattice constants in Table I result in the band structures shown in Fig. 3. The absence of the In 4*d* electrons in this explicit electronic-structure calculation gives rise to positive fundamental gaps even for the 2*H* and 3*C* polymorphs. The differences of $\Gamma_{1c}-\Gamma_{6v}$ (2*H*) and $\Gamma_{1c}-\Gamma_{15v}$ (3*C*) gaps with and without explicitly treating the In 4*d* electrons of about 0.76 or 0.79 eV can be interpreted as the shift of the VBM toward higher energies due to the overestimated *pd* repulsion in the *d*val description. In the *rs* polymorph with the much stronger nearest neighbor overlap the effect of the *pd* repulsion is with 0.09 eV negligibly small. The true percentage contribution of the *pd* repulsion may be estimated from the true position of the In 4*d* levels below the VBM. A rough value of this percentage may be obtained using perturbation-theory arguments, at least in the wurtzite case where experimental values of about 14.9 eV[63] and 16.7 eV[64] are available. They have to be compared with the DFT-LDA eigenvalue differences of 13.5 eV (in *d*val approach) or ∞ (in SIC with *d* electrons in the core). Fractions of $13.5/14.9 \approx 0.81$ or $13.5/16.7 \approx 0.91$ of the overestimated *pd* repulsion should be only taken into account. Such a procedure formally gives DFT-LDA gaps of −0.28(−0.21) eV (*zb*), −0.11(−0.04) eV (*w*), and 1.08(1.09) eV (*rs*) with a reliable inclusion of the *pd* repulsion. The strong effect of the semicore *d* electrons has also been found for other semiconductors, in particular II-VI compounds, but also for GaN.[69,71,72] We have to mention that there are other studies[22] which do

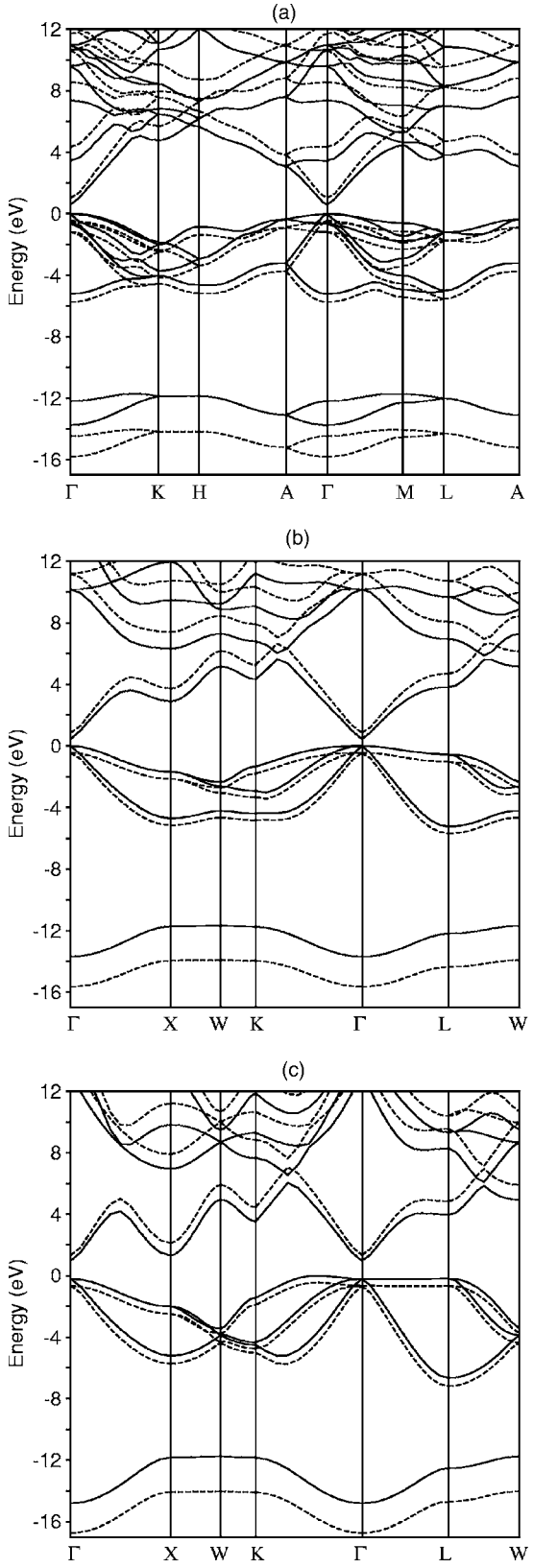

FIG. 3. Kohn-Sham (solid lines) and quasiparticle (dashed lines) band structures calculated with SIC pseudopotentials for three InN polymorphs: (a) wurtzite, (b) zinc blende, and (c) rocksalt. The In 4*d* electrons are frozen into the core. The lattice parameters of Table I have been used. The VBM is identified with the energy zero.

not find an indication for the *pd* repulsion. Rather, they claim that an "extra lowering of the bottom of the conduction band" is responsible for the negative or small gaps. However, these studies within an LCAO framework of the DFT-LDA found the In 4*d* bands about 15 eV below the VBM similar to the experimental data. They also calculate a 0.65 eV gap of *zb*-InN without the inclusion of quasiparticle effects.

The explicit inclusion or noninclusion of the In 4*d* electrons has also a remarkable influence on the crystal-field splitting Δ_{cr} in the case of *w*-InN. Without the *d* electrons, the energetical ordering of the valence-electron levels Γ_{6v} and Γ_{1v} at Γ is interchanged in Fig. 3. A negative crystal-field splitting $\Delta_{cr}=-43$ meV is observed. The *pd* repulsion is slightly different by less than 8% for Γ_{6v} and Γ_{1v}. The linear interpolation between the two DFT-LDA values for Δ_{cr} to a *pd* repulsion effect corresponding to the correct energetical distance VBM and In 4*d* gives small positive values of about 9.9 or 4.2 meV. Small positive Δ_{cr} values are in agreement with the experimental observations for the polarization dependence of the absorption edge with transitions from the Γ_{9v}, Γ_{7v}^{+}, and Γ_{7v}^{-} valence bands into the Γ_{7c} conduction band, if a spin-orbit splitting of the valence states of $\Delta_{so}=13$ meV[73] is assumed.

B. Band dispersion

Another interesting aspect of the band structures given in Fig. 3 is related to the band dispersion of the lowest conduction band in the case of the two InN polytypes 2*H* and 3*C*. The band structures revealed by the calculations indicate that the conduction-band minimum at the Γ point is much lower in energy than the conduction-band edge at other points in **k** space. This is a consequence of the above-mentioned large electron affinity of *w*-InN (and *zb*-InN). The next band minima are about 2.5 or even 3.0 eV above the minimum at Γ. This is in contrast to the other group-III nitrides AlN and GaN[62] and especially to other III-V semiconductors,[72] for which scattering of the hot carriers between different conduction-band valleys is widely allowed. The calculated band structures for *w*-InN and *zb*-InN have also consequences by fixing the branch point energy within the lowest conduction band.[74] This energy E_B also known as the charge neutrality level or the Fermi stabilization energy is defined as the crossover point from states higher in the gap that are mainly of conduction-band character (acceptor type) to states lower in energy that are mainly of valence-band character (donor type).[75] The branch point energy E_B is defined as the average midgap energy across the entire BZ. It can be determined by calculating the halfway point between the mean value of the lowest conduction band and the mean value of the highest valence band.[76] According to the SIC band structure in Fig. 3, such an estimate yields a value $E_B \approx 1.5$ eV above the VBM and, hence, in the lowest conduction band near the Γ point. Consequently, donor-type surface states should exist in the conduction band. These states can acquire positive charge by emitting their electrons into the conduction band. In a wurtzite (or zinc blende) crystal with surface charge, neutrality is achieved by accumulation of electrons close to the surface. We have to mention that a previous

TABLE II. Fundamental gap E_g at Γ in different approximations (i) DFT-LDA treating the In 4*d* electrons as valence electrons (*d*val), (ii) DFT-LDA with In 4*d* electrons frozen in the core but using SIC pseudopotentials (SIC), and (iii) perturbation-theory treatment of quasiparticle effects and correct inclusion of the *pd* repulsion (QP) for three InN polymorphs. In addition, the quasiparticle opening Δ^{QP} computed within the SIC approach is also listed. All values are given in units of eV. The two value for E_g (QP) are due to different contributions, 91 or 81% of the total *pd* repulsion (cf. text).

Polymorph	E_g (*d*val)	E_g (SIC)	Δ^{QP}	E_g (QP)
wurtzite	−0.21	0.58	0.93	0.82 (0.89)
zinc blende	−0.36	0.43	0.87	0.59 (0.67)
rocksalt	1.07	1.16	0.78	1.86 (1.87)

tight-binding calculation gave a value of $E_B=1.51$ eV,[77,78] and scanning tunneling spectrosocopy studies of *w*-InN surfaces yield a surface gap of about 1.3 eV,[79] also indicating the position of E_B in the lowest conduction band. Other indications for a pinning of the surface Fermi level in the conduction band region arise from photoemission and electron energy loss measurements.[42,65]

The characteristic dispersion of the lowest conduction band also allows the determination of an effective electron mass m^* near the bottom of the conduction bands at Γ, at least within the SIC approximation. Without quasiparticle corrections, we derive a value of $m^*=0.089m$ for the rocksalt structure. The band dispersion is enlarged for the other cubic polymorph, the zinc-blende structure. We derive an electron mass of $m^*=0.048m$. For the wurtzite InN the electron mass is anisotropic. The calculations for the directions $\Gamma A(m_{\parallel}^*)$ and $\Gamma M(m_{\perp}^*)$ result in the values $m_{\parallel}^*=0.059m$ and $m_{\perp}^*=0.069m$ slightly larger than the mass in the zinc-blende case. Also the anisotropy is rather small. For *w*-InN these theoretical values are somewhat smaller than measured masses. Measurements of the plasma frequency of the electrons and assuming a dielectric constant of $\varepsilon_\infty=6.7$,[7] resulted in an effective mass $m_{\perp}^*=0.07m$,[80] or $m_{\perp}^*=0.085m$.[81]

C. Influence of quasiparticle effects

The SIC approach gives a Kohn-Sham band structure also for the wurtzite and zinc-blende structures with positive fundamental gap (cf. Table II) and a correct energetical ordering of the bands (cf. Fig. 3). For that reason, the standard treatment of the quasiparticle effects described in Sec. II B can be applied. The input of the quasiparticle (QP) calculations in *GW* approximation[49] is dominated by the local electron density computed using the Kohn-Sham orbitals and the electronic dielectric constant ε_∞. The dielectric constants have been obtained within the independent-particle approximation (see discussion below). We found the values $\varepsilon_\infty(xx/yy)=7.03$ and $\varepsilon_\infty(zz)=7.41$ for wurtzite, $\varepsilon_\infty=7.92$ for zinc blende, and $\varepsilon_\infty=7.68$ for rocksalt. On average, a value $\varepsilon_\infty=7.16$ has been used in the self-energy calculation for the hexagonal polymorph. In the wurtzite case, the dielectric constants agree well with the values 7.16 and 7.27 calculated by Christensen and Gorczyca[14] but our zinc-blende constant exceeds their value. Persson *et al.*[34] computed values which are smaller or larger than ours in dependence of the used exchange-correlation potential. Experimental values are rare. An old measurement gave $\varepsilon_\infty=8.4$.[82] Recent experiments tend to a smaller value of about $\varepsilon_\infty=6.7$.[7] The general result is presented in Fig. 3. With respect to the VBM, the energy zero, all occupied bands are shifted toward lower energies (i.e., possess negative QP shifts), while all empty bands are pushed up toward higher energies (i.e., possess positive QP shifts). As a consequence, all optical transition energies between valence-band and conduction-band states are increased. All gaps are opened in comparison to the DFT-LDA band case.

The total quasiparticle corrections Δ^{QP} resulting for the fundamental gaps of the polymorphs under consideration are also given in Table II. The gap openings of 0.8–0.9 eV are similar to those values 0.80 eV[70] and 1.03 eV[34] estimated by means of the semiempirical Bechstedt-Del Sole formula.[67] Together with the Kohn-Sham gap resulting from an extrapolation of the *pd* repulsion (see Sec. III B), in Table II, one obtains values for the fundamental quasiparticle gap of about $E_g(QP)=0.8$ eV(*w*), 0.6 eV(*zb*), and 1.9 eV(*rs*). In the wurtzite case, the computed value excellently agrees within the accuracy of the modern electronic-structure theory of ~0.1–0.2 eV with recent experimental values. The analysis of optical absorption, photoluminescence (PL), photoluminescence excitation, and photoreflectivity data obtained on single crystalline hexagonal InN films grown by MBE leads to a true band gap of *w*-InN of $E_g\approx 0.7$ eV.[1,83] Good coincidence of data for optical absorption edge, PL peak energy, and photomodulated reflectance for MBE grown layers also tend to $E_g\approx 0.7$ eV after correction of the Burstein-Moss shift.[2] Matsuoka *et al.*[3] observed at room temperature PL at 0.76 eV and an absorption edge at 0.7–1.0 eV for MOVPE-grown InN films. Spectroscopic ellipsometry studies also indicate a value of the onset of the optical absorption at about 0.75 eV[6,8] or even 0.65 eV for vanishing free-carrier concentration.[7] A reliable experimental value for the zero-temperature gap of 2*H*-InN could be 0.69 eV.[84] Electronic structure calculations for InN including many-body effects to model the excitation aspect are rather rare. The use of an exact KS exchange potential gives a gap value of about $E_g=1.4$.[36] However, this method seems to overestimate the gaps for normal-gap semiconductors. In the Si case, the overestimate amounts to 0.3 eV. A new all-electron, augmented-wave implementation of the *GW* approximation using eigenfunctions generated by a full-potential linearized muffin-tin orbital (LMTO) method[30] leads to a quasiparticle gap $E_g(QP)\approx 0.05$ eV. Recently the same authors[85] suggested a different result of $E_g(QP)\approx 0.5$ eV for the zinc-blende structure.

The band structures given in Fig. 3 suffer from the absence of the In 4*d* electrons, in particular the *pd* repulsion as discussed for the Γ_{15v} and Γ_{6v}/Γ_{1v} valence-band maxima above. For instance, an occupied *p*-like state in Fig. 3 has to be pushed toward higher energies by 0.69(or 0.62) eV (see above discussion). However, such a shift is not valid for the other bands. In order to obtain a more or less correct description of the *pd* repulsion for a given band ν and a given $\mathbf{k}$

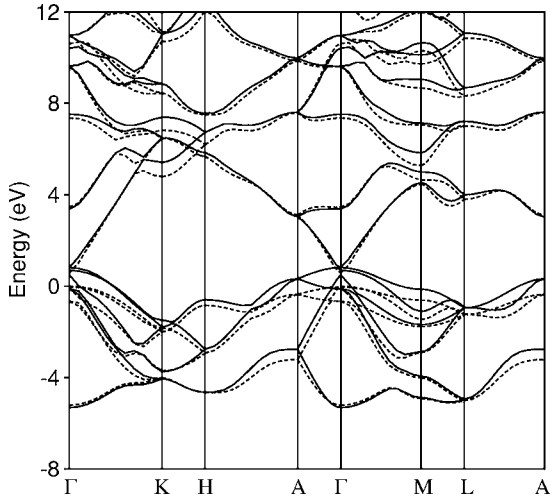

FIG. 4. Comparison of the Kohn-Sham band structures of *w*-InN calculated in the approximations *d*val (solid lines) and SIC (dashed lines). The alignment has been made for the lowest conduction band at the *A* point.

point within the BZ, we compare the two Kohn-Sham band structures obtained within the *d*val and the SIC approach. This is shown in Fig. 4 in the case of the wurtzite polymorph. The alignment of the two band structures is made widely for the lowest conduction band in the **k**-space regions where (apart from the Γ point itself) it is strongly *s*-like. Explicitly, we use the *A* point for alignment of the lowest conduction bands, but correct this alignment so that only 81% (see above) of the uppermost-valence-band shift between *d*val and SIC approximation is really taken into account. This procedure results in a shift of the uppermost valence bands against each other of about 0.6 eV. For all valence bands and the lowest conduction bands, the results are given in Table III for high-symmetry points in the hexagonal BZ and in Fig. 5 along high-symmetry lines. The valence-band maximum at Γ has been modified according to the discussion above. In addition, the eigenvalues corrected by their QP shifts in *GW* approximation, i.e., the QP energies, are listed. The absolute QP shifts for the valence bands vary between −0.45 eV to −2.29 eV from the first to the eighth valence band. The conduction-band shifts increase from 0.44 eV($c1$) to 1.37 eV($c8$). The resulting QP values

TABLE III. Bloch energies of the lowest eight conduction ($c1-c8$) and highest eight valence ($v1-v8$) bands of *w*-InN at high-symmetry points in the BZ. The Kohn-Sham eigenvalues are taken from a SIC calculation but slightly modified by 81% of the *pd* repulsion extracted from a comparison of the results of SIC and *d*val calculations (cf. text). The addition of the quasiparticle shifts in *GW* approximation (based on SIC wave functions) gives the QP energies. The top of the KS valence bands (Γ_{6v}) is defined as energy zero. All values are in eV.

Band		$v8$	$v7$	$v6$	$v5$	$v4$	$v3$	$v2$	$v1$
Γ	KS	−14.47	−12.91	−5.96	−0.88	−0.88	−0.08	0.00	0.00
	QP	−16.53	−15.17	−6.48	−1.42	−1.42	−0.54	−0.52	−0.52
K	KS	−12.60	−12.60	−4.70	−4.70	−4.39	−2.48	−2.48	−2.21
	QP	−14.90	−14.90	−5.22	−5.22	−4.86	−2.97	−2.97	−2.72
M	KS	−13.00	−12.47	−5.54	−4.61	−3.53	−2.35	−1.82	−0.88
	QP	−15.24	−14.79	−6.06	−5.15	−4.02	−2.88	−2.27	−1.42
A	KS	−13.81	−13.81	−3.49	−3.49	−0.45	−0.45	−0.45	−0.45
	QP	−15.93	−15.93	−4.03	−4.03	−0.99	−0.99	−0.99	−0.99
H	KS	−12.58	−12.58	−5.29	−5.29	−3.44	−3.44	−1.30	−1.30
	QP	−14.89	−14.89	−5.80	−5.80	−3.91	−3.91	−1.83	−1.83
L	KS	−12.73	−12.73	−5.61	−5.61	−1.66	−1.66	−1.63	−1.63
	QP	−15.01	−15.01	−6.14	−6.14	−2.19	−2.19	−2.14	−2.14
Band		$c1$	$c2$	$c3$	$c4$	$c5$	$c6$	$c7$	$c8$
Γ	KS	−0.14	2.73	6.83	8.97	8.97	9.80	10.32	10.32
	QP	0.30	3.63	8.03	10.01	10.01	10.89	11.57	11.57
K	KS	4.64	5.82	5.82	6.63	8.13	8.13	10.30	10.38
	QP	5.56	6.92	6.92	7.76	9.40	9.40	11.68	11.65
M	KS	3.86	4.26	5.07	6.46	8.32	9.39	9.93	11.42
	QP	4.79	5.21	6.12	7.63	9.62	10.49	11.31	12.95
A	KS	2.38	2.38	6.95	6.95	9.30	9.30	9.30	9.30
	QP	3.11	3.11	8.17	8.17	10.40	10.40	10.40	10.40
H	KS	5.16	5.16	5.97	5.97	6.90	6.90	11.81	11.81
	QP	6.18	6.18	7.08	7.08	8.12	8.12	13.08	13.08
L	KS	3.30	3.30	6.52	6.52	7.96	7.96	10.38	10.38
	QP	4.22	4.22	7.72	7.72	9.21	9.21	11.75	11.75

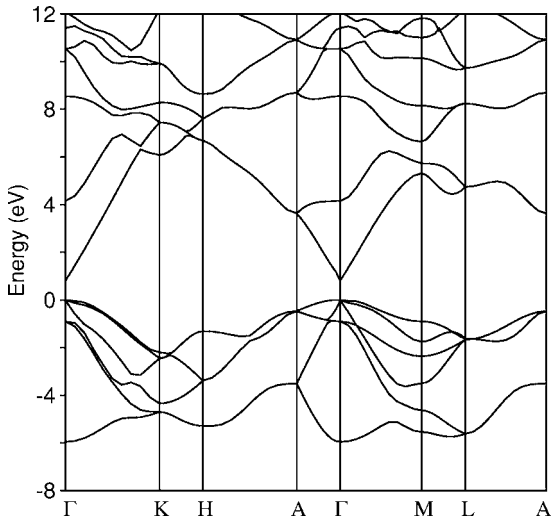

FIG. 5. Quasiparticle band structure of *w*-InN. The inclusion of the *pd* repulsion is described in the text. The valence-band maximum is taken as energy zero.

are in rough agreement with results of empirical-pseudopotential calculations,[39] which, however, have assumed our calculated gaps to fit the pseudopotential coefficients. The most important conclusions from Table III are the energy differences $\Gamma_{1c}-\Gamma_{6v}$ (fundamental gap) of about 0.82 eV and $\Gamma_{6v}-\Gamma_{1v}$ (crystal-field splitting) of about 0.02 eV using the *pd* repulsion and the quasiparticle corrections described in the text.

From band structures including quasiparticle corrections, we can derive effective masses as well. Unfortunately, numerical noise in conjunction with the extreme nonparabolicity of the bands makes reliable polynomial fits of the conduction band dispersion difficult. In contrast to the DFT case, for *GW* band structures the result depends strongly on the chosen fit polynomial. A too low order of the polynomial results in a too bad description of the nonparabolicity, a too high order of the polynomial fits (increased) numerical noise only. Therefore, we have to make a compromise in the form of a polynomial fit of the sixth order. Such a fit gives still values in the DFT-LDA case which are not too far from well-converged values obtained with more precise higher-order polynomials. We derive for the two approximations DFT-LDA (*GW*) effective masses $m^*_{\parallel}=0.062m$ ($m^*_{\parallel}=0.089m$) and $m^*_{\perp}=0.088m$ ($m^*_{\perp}=0.131m$) in the wurtzite case, $m^*=0.059m$ ($m^*=0.119m$) in the zinc-blende case, and $m^*=0.092m$ ($m^*=0.061m$) in the rocksalt case. Although the numerical error bar in the quadratic fit coefficient for the *GW* conduction band is at least 30%, the overall trend (larger effective masses in the wurtzite and zinc-blende case, smaller mass in the rocksalt case) is also confirmed for other choices of the fit polynomials (in all cases an increase of the order of the polynomial results in even larger discrepancies between DFT-LDA and *GW* effective masses). The overall picture is partly changed after inclusion of quasiparticle corrections. Still, *GW* calculations yield very small masses compared to most other semiconductors and a still moderate (although somewhat larger) anisotropy in the wurtzite case. The calculated values are now larger than the measured ones. The findings of the smallest effective mass for the zinc-blende polytype seems to be not true within the quasiparticle framework. The *GW* zinc-blende mass now tends toward the *GW* basal-plane wurtzite mass, and the *GW* wurtzite mass parallel to the *c* axis becomes smaller than the zinc-blende mass. Surprisingly, the *GW* rocksalt mass now becomes the smallest one, whereas in DFT-LDA, we find the rocksalt mass to be the largest one among all polymorphs.

V. DIELECTRIC FUNCTION

A. General line shape

The independent-particle approximation[41] is a good starting point for the calculation of the complex dielectric function $\varepsilon(\omega)$ for the cubic polymorphs of InN or the two independent tensor components $\varepsilon_{xx}(\omega)=\varepsilon_{yy}(\omega)$ and $\varepsilon_{zz}(\omega)$ in the hexagonal case. It leads to the Ehrenreich-Cohen formula.[86] In a first approach, we use the eigenfunctions and eigenvalues of the SIC approach. As shown above, it gives the correct ordering of the energy bands. Moreover, despite the neglect of the quasiparticle effects, the fundamental gaps have to increase only by 0.24 eV(*w*), 0.16 eV(*zb*), or 0.70 eV(*rs*) to obtain the quasiparticle gap because of the wide compensation of the gap shrinkage due to the *pd* repulsion and the gap opening by the *GW* corrections for the wurtzite and zinc-blende crystals. The imaginary part of the dielectric functions is related to a **k**-point summation over Dirac's δ functions. The tetrahedron method[87] is applied to the corresponding BZ integration employing 256 (cubic case) and 910 (hexagonal case) **k** points in the irreducible part of the BZ. The real part of the dielectric function then follows from a Kramers-Kronig relation.[41] The resulting spectra are presented in Fig. 6. Of course, the effect of the quasiparticle shifts on the higher interband transitions as well as the excitonic effects have to be discussed subsequently in separate studies.

For *w*-InN and *zb*-InN, the imaginary parts of the dielectric functions show a characteristic line shape that in a weaker form also appears for the rocksalt polymorph because of the larger fundamental gap (cf. Fig. 6). After a steep onset of the light absorption in the frequency range somewhat above E_g(SIC) (Table II), it follows a rather constant, plateau-like behavior until photon energies of about 4.0 eV(*zb*) or 4.5 eV(*w*). The transition region around 1 eV or somewhat above is well pronounced for the 3*C* and 2*H* structures. In the wurtzite case, it looks like a kink and even becomes a peak structure for *zb*-InN. The *zz* component of the dielectric function already exhibits a small peak in this frequency region. In the high-energy region between 3 and 12 eV characteristic peaks occur. They are specific for the considered polymorph. Large differences are even between the 3*C* and 2*H* polytypes of InN, although they only differ in the stacking of the In—N bilayers in [111]/[0001] direction. Seemingly, all these peaks should be related to optical interband transitions at critical points in the BZ. We will discuss this relationship below. In the wurtzite case, there are characteristic changes between the ordinary (xx,yy) and extraordinary (zz) components of the dielectric tensor. This aniso-

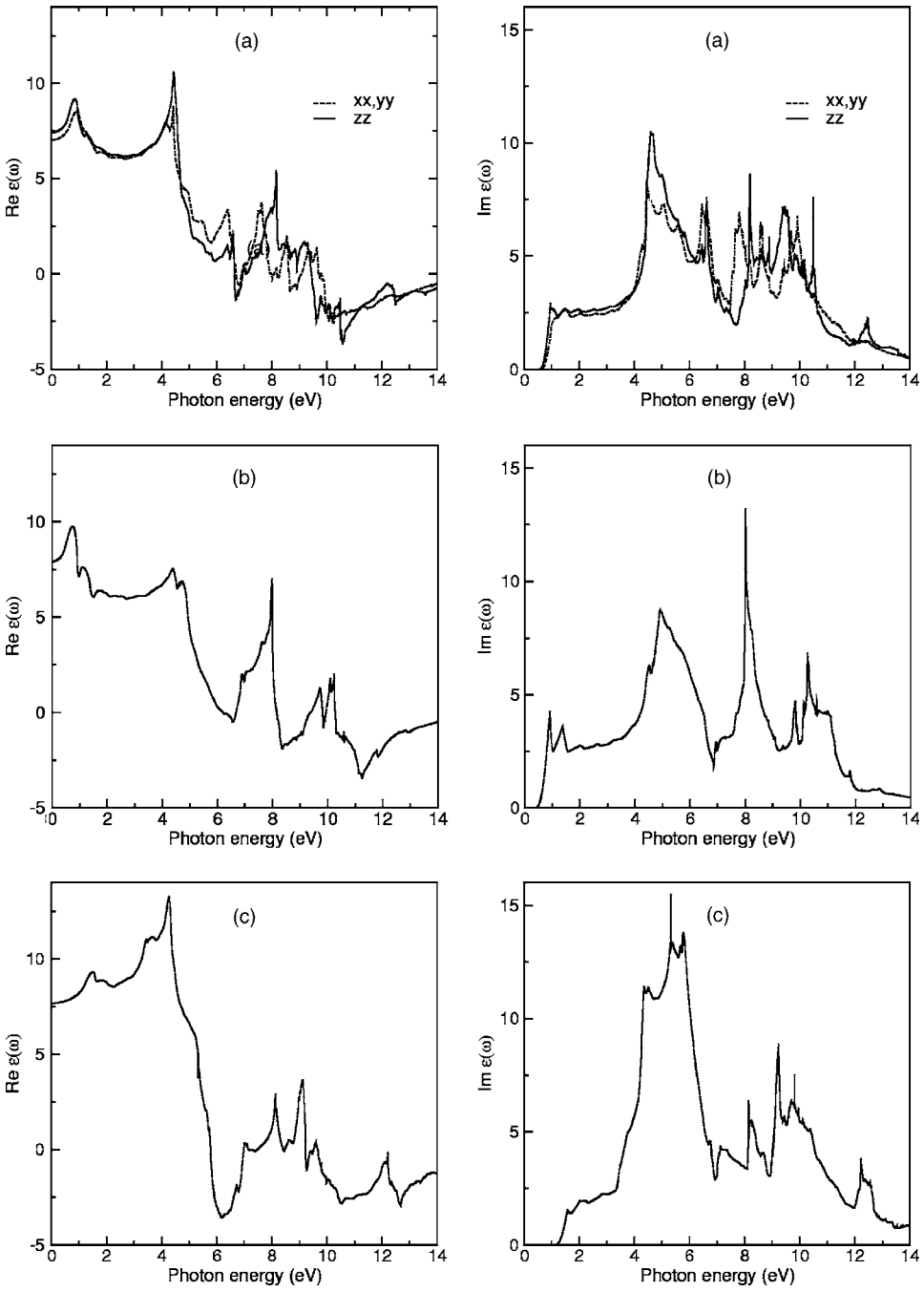

FIG. 6. Real part and imaginary part of the dielectric function of InN crystallizing in (a) wurzite, (b) zinc-blende, and (c) rocksalt structure. In the hexagonal case, both independent tensor components (solid and dashed lines) are shown. The calculations have been performed within the independent-particle approximation using PAW-SIC pseudopotentials.

tropy is observable in the entire frequency region. The characteristic line shape of the imaginary part of the dielectric function is independent of the theoretical approach used (at least in the single-particle picture),[14,34] at least for 3*C* and 2*H*. The main variations concern the details of the peaks in the high-energy region assigned to interband transitions at critical points. They are dominated by optical transitions near high-symmetry points in the BZ far from the BZ center. For wurtzite InN, Table IV summarizes optical interband energies at high-symmetry points in quasiparticle quality together with the relative strengths of these transitions. The optical polarization anisotropy is clearly visible in Table IV and Fig. 6(a). The experimental spectra measured for *w*-InN[6–8] exhibit the same characteristic behavior of the line shape. Only the peak positions and the number of peaks in the high-energy region differ. Lifetime broadening and sample quality obviously influence the spectra. However, the measurements[8] also show the drastic anisotropy in the range of the interband transitions. This holds in particular for the main peak structure in the 4.5–5.5 eV range in Fig. 6(a), whose energetical positions with a maximum at 5.4 eV are not too far from the calculations including many-body effects. In addition, the absolute value of $\mathrm{Im}\,\varepsilon(\omega) \approx 2.5$ in the plateau region[6–8] is also reproduced.

The principal frequency dependence of the real part of the dielectric functions $\mathrm{Re}\,\varepsilon(\omega)$ in Fig. 6 does not vary much with the polymorph. The spectra show characteristic maxima for photon energies somewhat above the fundamental gap E_g

TABLE IV. Optical transition energies (in eV) including quasiparticle effects and *pd* repulsion and kinetic-energy equivalents $T_j=1/2m|\langle \nu\mathbf{k}|p_j|c\mathbf{k}\rangle|^2$ ($j=x/y$ or z) of the optical transition matrix elements (in meV) at high-symmetry points in the Brillouin zone for *w*-InN. In the case of identical transition energies the sum of the matrix elements is listed. Transitions which are forbidden or extremely weak ($\Sigma_j T_j \leqslant 100$ meV) or have transition energies $\geqslant 10$ eV are not given.

High-Symmetry Point	Optical Transition $v_i \rightarrow c_j$	Transition Energy	Transition Matrix Element $T_{x/y}$	Transition Matrix Element T_z
Γ	$v1,v2\rightarrow c1$	0.82	2303	0
	$v3\rightarrow c1$	0.84	0	2478
	$v4,v5\rightarrow c2$	5.05	3304	0
K	$v1\rightarrow c1$	8.28	0	2898
	$v2,v3\rightarrow c1$	8.53	1660	0
	$v1\rightarrow c2,c3$	9.64	590	0
	$v2,v3\rightarrow c2,c3$	9.89	48	1985
M	$v1\rightarrow c1$	6.21	1765	0
	$v2\rightarrow c1$	7.06	0	691
	$v3\rightarrow c2$	8.09	3093	0
	$v2\rightarrow c3$	8.39	0	202
	$v4\rightarrow c2$	9.23	0	262
A	$v1-v4\rightarrow c1,c2$	4.10	4174	0
	$v5,v6\rightarrow c1,c2$	7.14	0	396
	$v1-v4\rightarrow c3,c4$	9.16	1455	0
H	$v1,v2\rightarrow c1,c2$	8.01	1420	8834
	$v1,v2\rightarrow c3,c4$	8.91	304	0
L	$v1,v2\rightarrow c1,c2$	6.36	682	3003
	$v3,v4\rightarrow c1,c2$	6.41	2741	0
	$v1,v2\rightarrow c3,c4$	9.86	816	2286
	$v3,v4\rightarrow c3,c4$	9.91	2210	0

at about 4.5 eV. In the energy range 6–10 eV, each real part has several zeros which may be related to longitudinal excitons. These zeros are much below the plasma frequency of the valence electrons of InN which should be around 19.0 eV(zb,w) or 21.1 eV(rs). The values $\varepsilon_\infty=\mathrm{Re}\,\varepsilon(0)$ give the high-frequency electronic dielectric constants discussed above. Their values $\varepsilon_\infty=7-8$ vary only weakly with the polymorph.

B. Absorption edge

At least for *w*-InN and *zb*-InN, the band structures in Fig. 3 indicate that for photon energies $\hbar\omega \lesssim 4$ eV the optical absorption coefficient, $\alpha(\omega)\sim \mathrm{Im}\,\varepsilon(\omega)$, should be dominated by optical transitions from the three highest valence bands v_1, v_2, and v_3 into the lowest conduction band c near the Γ point. This fact suggests a description of the dielectric function in this frequency range by a four-band $\mathbf{k}\cdot\mathbf{p}$ Kane model.[80,88] The strong dispersion should be related to strong coupling of the conduction and valence states due to a small fundamental gap E_g. For a rough description, we neglect the small spin-orbit interaction constant and crystal-field splitting (in the 2*H* case) of the order of 10 meV (Sec. IV B and Ref. 73). Consequently, the zinc-blende and wurtzite cases are nearly described in the same manner taking into account only the *s*-like Γ_{1c} and *p*-like Γ_{15v} levels with a real effective coupling constant $P=(\hbar/im)\langle s|p_x|x\rangle$ between the $|s\rangle$ and $|x\rangle$, $|y\rangle$, and $|z\rangle$ states mediated by the momentum operator. With $E_k=\hbar^2k^2/2m$ the corresponding $\mathbf{k}\cdot\mathbf{p}$ Hamiltonian is given as[89]

$$\begin{pmatrix} E_g+E_k & iPk_x & iPk_y & iPk_z \\ -iPk_x & E_k & 0 & 0 \\ -iPk_y & 0 & E_k & 0 \\ -iPk_z & 0 & 0 & E_k \end{pmatrix}. \tag{1}$$

With $E_p=(2m/\hbar^2)P^2$, this Hamiltonian gives rise to the Bloch bands

$$E_{c/v_2}(\mathbf{k})=\frac{1}{2}\left[E_g \pm \sqrt{E_g^2+4E_pE_k}\right]+E_k,$$

$$E_{v_1/v_3}(\mathbf{k})=E_k. \tag{2}$$

The bands are isotropic, but two of them exhibit a strong nonparabolicity which will be identified as the reason for the characteristic line shape of Im $\varepsilon(\omega)$. Despite this nonparabolicity of the conduction band, an effective electron mass can be defined at Γ by

$$\frac{m^*}{m}=\frac{1}{1+E_p/E_g}. \tag{3}$$

With an experimental gap value of $E_g=0.7$ eV, one derives electron masses of $m^*=0.045-0.065m$ for characteristic matrix elements of the momentum operator of $E_p=10-15$ eV. These values approach those measured or derived from the band structures in Fig. 3 (cf. discussion in Sec. IV C). The eigenfunctions of the Hamiltonian (1) lead directly to the matrix elements of the optical transition operator between conduction-band ($|c\mathbf{k}\rangle$) and valence-band ($|v_i\mathbf{k}\rangle, i=1,2,3$) states,

$$\langle c\mathbf{k}|\mathbf{p}|v_2\mathbf{k}\rangle=-\frac{m}{\hbar}P\frac{\mathbf{k}}{|\mathbf{k}|},$$

$$\langle c\mathbf{k}|\mathbf{p}|v_i\mathbf{k}\rangle=\frac{im}{\hbar}P\left\{\frac{1}{2}\left[1+\frac{E_g}{\sqrt{E_g^2+4E_pE_k}}\right]\right\}^{1/2}\mathbf{n}_i \tag{4}$$

with orthonormal vectors $\mathbf{n}_i=\mathbf{n}_i(\mathbf{k})$ ($i=1,3$) perpendicular to $\mathbf{k}$.

These matrix elements enter the Ehrenreich-Cohen formula for the three optical transitions involved. Using the trace of the tensor $\varepsilon(\omega)=\frac{1}{3}[\varepsilon_{xx}(\omega)+\varepsilon_{yy}(\omega)+\varepsilon_{zz}(\omega)]$, one finds for the imaginary part

$$\mathrm{Im}\,\varepsilon(\omega) = \left(\frac{2\pi e}{m\omega}\right)^2 2 \int \frac{d^3\mathbf{k}}{(2\pi)^3} \sum_{i=1}^{3} \frac{1}{3} \sum_{j=1}^{3} |\langle c\mathbf{k}|p_j|v_i\mathbf{k}\rangle|^2 \times \delta[E_c(\mathbf{k}) - E_{v_i}(\mathbf{k}) - \hbar\omega]. \quad (5)$$

By means of expressions (2) and (4) the **k**-space integration leads to

$$\mathrm{Im}\,\varepsilon(\omega) = \frac{1}{3}\left(\frac{e^2}{2a_B E_p}\right)^{1/2} \sqrt{1-x}[\sqrt{1+x}+8]\theta(1-x)|_{x=E_g/\hbar\omega}, \quad (6)$$

where a_B is the Bohr radius. Close to the fundamental gap $\hbar\omega \gtrsim E_g$, the frequency dependence of the imaginary part of the dielectric function is given by the square-root behavior $\mathrm{Im}\,\varepsilon(\omega) \sim \sqrt{\hbar\omega - E_g}$ as known for parabolic bands. Far away from the absorption onset, $\hbar\omega \gg E_g$, a constant $\mathrm{Im}\,\varepsilon(\omega) = 3(e^2/2a_B E_p)^{1/2}$ is obtained. This explains the plateau-like character of the observed dielectric function in the frequency range 1.5–4.0 eV. Interestingly, the absolute value $\mathrm{Im}\,\varepsilon(\omega) \approx 2.86$–$3.50$ for $E_p = 10$–15 eV is also well reproduced in comparison to the *ab initio* calculations in Fig. 6 and the measurements.[6–8] The deviations of the frequency dependence in (6) from the square-root behavior are due to the nonparabolicity of the band structure (2). Consistently, we state that the plateau observed in the frequency dependence of the imaginary part of the dielectric function is a consequence of the nonparabolicity of the bands, in particular, of the conduction band and the light-hole band, near the fundamental gap. Unfortunately, formula (6) cannot explain the kink near $\hbar\omega \approx 2E_g$. For this purpose, the chosen electronic-structure model is too simple.

C. Influence of excitonic effects

The excitonic effects have been included in the dielectric functions of *w*-InN using the initial-value formulation described elsewhere.[55,56] The starting point of such a calculation is the electron-hole pair Hamiltonian. Its diagonal elements without Coulomb effects are derived from the quasiparticle energies including the *pd* repulsion as described above (see also Table IV). We calculate the corresponding energy differences at 4704 MP **k** points in the hexagonal BZ. According to our experiences, this gives well-converged spectra for other semiconductors. In contrast to the independent-particle or independent-quasiparticle approximation, the tetrahedron method cannot be applied. A wave vector does not represent a set of good quantum numbers to describe the internal motion of the electron-hole pairs. Taking into account a lifetime broadening of 0.2 eV for each pair, the real part and the imaginary part of the dielectric function are directly computed. Their calculation in a wide range of photon energies up to 9 eV requires at least eight valence bands and eight conduction bands. The matrix elements of the (electron-hole) exchange interaction and the screened Coulomb attraction are computed by means of the wave functions from the PAW-SIC approximation. The screening function is the same as used in the quasiparticle calculations.

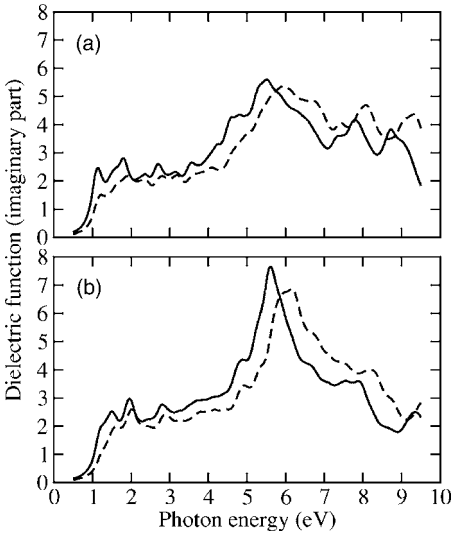

FIG. 7. Imaginary part of the dielectric function of *w*-InN for Coulomb-correlated electron-hole pairs (solid lines) and independent quasiparticles (dashed lines). The ordinary and extraordinary functions are given in the upper (a) and lower (b) panel, respectively.

In Fig. 7, we demonstrate the influence of the excitonic effects on the imaginary part of both the ordinary and extraordinary dielectric function for wurtzite InN. Apart from small shifts in the energetical positions, the quasiparticle spectra also show other discrepancies with respect to those in Fig. 3(a). Because of the used lifetime broadening, fine structures in the spectra disappear and there is no sharp onset of the optical absorption at the energy gap given in Table II. Instead of the plateau-like behavior in the energy region 1–4 eV, the spectra in Fig. 7 exhibit small peaks. They are consequences of the not completely converged calculations with respect to the number of **k** points. The numerical difficulty is to generate a constant spectrum by summing up over a finite number of lifetime-broadened Dirac's δ functions. However, in the higher-frequency region above 4 eV, the computed spectra are reasonably converged.

In the low-energy region $\hbar\omega \lesssim 4$ eV, one only observes a weak influence of the excitonic effects. There is a small Coulomb enhancement of about 10%. Exciton bound states below the fundamental gap do not occur in our calculation. They may be generated by restricting to a few band pairs and an extremely high density of **k** points around Γ.[53,57] However, the current sample quality does not allow optical measurements for samples with a free electron concentration below 10^{17} cm^{-3}, i.e., below the Mott density.[90] The energy region 4–9 eV is characterized by a substantial redshift of about 0.5 eV with a few exceptions, e.g., the shoulder near 4.8 eV in the extraordinary case. In addition, a redistribution of spectral strength from higher to lower photon energies happens. This effect is obvious for the extraordinary dielectric function. The higher energy peak at 7.9 eV looses 8% intensity while the low-energy peak at 5.6 eV increases its intensity by the same value due to the Coulomb coupling of independent quasielectron-quasihole pairs. Similar effects have been observed for the E_1 and E_2 peaks of diamond and zinc-blende semiconductors.[51–53,55,56]

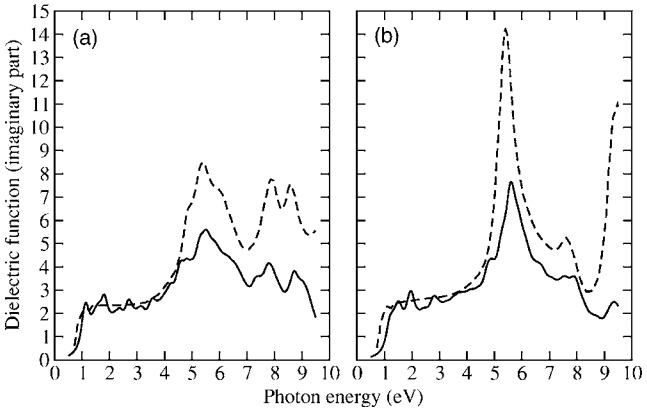

FIG. 8. Comparison of calculated (solid lines) and measured (dashed lines) imaginary parts of the ordinary (a) and extraordinary (b) dielectric function of *w*-InN. The experimental spectra have been obtained using spectroscopic ellipsometry for room temperature (Refs. 6 and 8).

Despite the high-electron concentrations $7.7\times10^{17}-1.4\times10^{19}$ cm^{-3} of the MBE-grown samples studied by means of spectroscopic ellipsometry at room temperature,[6–8] the resulting dielectric functions can directly be compared with the calculated spectra in Fig. 7. Only the absorption edge itself is influenced by the free carriers, mainly by the Burstein-Moss effect.[90] However, it has been shown experimentally that the energetical positions of the high-energy peaks, e.g., in the range 4.8–6.2 eV, of the dielectric function remain almost uninfluenced by a variation of the free-electron concentration.[7] Such a comparison with measurements of Goldhahn *et al.*[6,8] is shown in Fig. 8. This figure demonstrates an excellent agreement of theory and experiment. This is, in particular, valid for the principal line shape of the imaginary part, steep increase of the optical absorption below 1 eV, the plateau region 1–4 eV (with some wiggling in the theoretical spectra due to the finite number of **k** points), and the same peak structure in the high-energy region 4–9 eV. The agreement concerns the spectral strengths (at least in the low-energy region), the peak positions and the overall optical anisotropy. Deviations only concern the spectral strengths of the main absorption peaks in the ordinary and extraordinary spectra above 5 eV, whereas the plateau region with $\mathrm{Im}\,\varepsilon(\omega)\approx2.5$ is rather equal. In particular, the height of the central peak in the extraordinary spectrum[8] is surprisingly underestimated in the theory. The situation is much better in the ordinary case,[6,8] in particular for the comparison with results of Kasic *et al.*[7] who also find a peak maximum at about $\hbar\omega=5.4$ eV near $\mathrm{Im}\,\varepsilon(\omega)=6$, i.e., much closer to the theoretical predictions than Refs. 6 and 8. The disagreement in the intensities does not occur for other semiconductors[51–53,55,56] and, hence, needs future discussions. Around $\hbar\omega\approx9$ eV, the calculations underestimate the spectral strength because of the neglect of higher optical transitions which may be redistributed to lower energies due to the Coulomb effects. However, the discrepancies between the results of two spectroscopic ellipsometry experiments[7,8] for the intensities of the ordinary spectrum also indicate experimental uncertainties in the determination of the absolute values of the dielectric function for thin layers.

TABLE V. Positions of the main high-energy spectral features in the imaginary part of the dielectric functions (DFs) obtained from calculation or spectroscopic ellipsometry (Refs. 7 and 8). All values in eV.

	Ordinary DF			Extraordinary DF	
Spectral Feature	Calc.	Ref. 8	Ref. 7	Calc.	Ref. 8
shoulder	4.7	4.88	4.84	4.8	
peak	5.5	5.35	5.41	5.6	5.38
shoulder	6.1	6.05	5.59/6.10	6.7	
peak	7.8	7.87		7.6/7.9	7.63
peak	8.7	8.60		9.4	9.44

The number of the high-energy peaks and the line shape are in very good agreement between computed and measured spectra. One has to consider that the calculations are really parameter free, including the use of theoretical lattice constants. The good agreement is also demonstrated in Table V with an inaccuracy of the *ab initio* calculations of about 0.1–0.2 eV with respect to the peak positions in the dielectric functions. In the ordinary case, the main peak possesses two shoulders, the high-energy one is rather broad. It follows two further peaks with somewhat lower spectral strength. The measured and calculated peak positions deviate by less than 0.1 eV. In the extraordinary case, the pronounced central peak at $\hbar\omega\approx5.4$ eV (experimental position, see Fig. 8) is followed by two other structures. While the peak near 7.6 eV (experiment[8]) agrees well with respect to the position (double peak at 7.6/7.9 eV in the calculated spectrum), the spectral strengths vary between 5.2 and 3.6 between experiment and theory. The highest energy peaks occur at nearly the same position $\hbar\omega\approx9.4$ eV in the theoretical and experimental spectra but differ remarkably in their intensity. Reasons may be related to experimental problems in this photon-energy region and the neglect of the Coulomb coupling to electron-hole pairs with higher energies discussed above. However, another nice agreement with the experiment has to be mentioned. The overall optical anisotropy agrees qualitatively. In the plateau region and at the main peak, the extraordinary spectrum has a larger intensity. For energies above $\hbar\omega=6$ eV, the opposite effect occurs. The ratios of ordinary and extraordinary spectra (not shown here) show a similar spectral variation for both the measurement and the calculation.

VI. SUMMARY AND CONCLUSIONS

Using a combination of an *ab initio* density functional theory for the ground-state properties and the many-body perturbation theory to describe electronic excitations, we have calculated properties of the III-V semiconductor InN crystallizing in three different crystal structures, wurtzite, zinc blende, and rocksalt. The calculated energetical ordering of the polymorphs and the transition pressure for the pressure-induced transition from the wurtzite into the rock-

salt structure agree well with the experimental observations. The calculated lattice constants of the 2*H* and 3*C* polytypes suffer somewhat from the overbinding tendency due to the treatment of exchange and correlation within the local density approximation.

The In 4*d* electrons play a crucial role not only for the correct structural properties, but also in the electronic structure. The application of the DFT-LDA leads to an underestimate of the energetical distance of valence *p* electrons and In 4*d* states. The consequence in the wurtzite and zinc-blende cases is a wrong energetical ordering of the *s*-like antibonding and *p*-like bonding states. In order to correct the overestimated *pd* repulsion, we also performed calculations where the In 4*d* electrons have been frozen into the core. The wave functions and eigenenergies of these calculations allow us the treatment of the quasiparticle effects within the standard perturbation-theory scheme. Band structures of the valence electrons have been derived that account for the excitation aspect and the *pd* repulsion correctly on the energy scale with an inaccuracy of 0.1–0.2 eV. We predict fundamental energy gaps of about 0.8 (wurtzite), 0.6 (zinc blende), and 1.9 eV (rocksalt). The wurtzite value is in agreement with recent measurements. The role of the low-lying conduction band minimum for *w*-InN and *zb*-InN for the large electron affinity and for the charge neutrality level in the conduction-band region has been discussed.

Independent of the full inclusion of excitonic effects or not the optical spectra, more strictly speaking the imaginary parts of the dielectric functions, show a characteristic line shape. A steep onset of the absorption is followed by a plateau-like region (which is less pronounced for rocksalt because of the larger fundamental gap). In the high-energy region, a characteristic peak structure has been observed. The plateau region has been traced back to the strong nonparabolicity of the bands (in particular, the conduction band) near the Γ point in the Brillouin zone. As a consequence of the step-like line shape and the almost frequency independence in the plateau region, excitonic effects play a weaker role in the lower frequency region as expected. On the other hand, the electron-hole interaction couples several interband transitions and leads to a redshift of the quasiparticle spectrum and a redistribution of oscillator strength toward lower energies.

ACKNOWLEDGMENTS

We would like to thank R. Goldhahn for valuable discussions. The authors acknowledge financial support from the Deutsche Forschungsgemeinschaft (Project No. Be 1346/18-1) and European Community in the framework of the network of excellence NANOQUANTA (Contract No. NMP4-CT-2004-500198).

[1] V. Yu. Davydov, A. A. Klochikhin, R. P. Seisyan, V. V. Emtsev, S. V. Ivanov, F. Bechstedt, J. Furthmüller, H. Harima, A. V. Mudryi, J. Aderhold, O. Semchinova, and J. Graul, Phys. Status Solidi B **229**, R1 (2002).

[2] J. Wu, W. Walukiewicz, K. M. Yu, J. W. Ager III, E. E. Haller, H. Lu, W. J. Schaff, Y. Saito, and Y. Nanishi, Appl. Phys. Lett. **80**, 3967 (2002).

[3] T. Matsuoka, H. Okamoto, M. Nakao, H. Harima, and E. Kurimoto, Appl. Phys. Lett. **81**, 1246 (2002).

[4] T. L. Tansley and C. P. Foley, J. Appl. Phys. **59**, 3241 (1986).

[5] T. V. Shubina, S. V. Ivanov, V. N. Jmerik, D. D. Solnyshkov, V. A. Vekshin, P. S. Kopév, A. Vasson, J. Leymarie, A. Kavokin, H. Amano, K. Shimono, A. Kasic, and B. Monemar, Phys. Rev. Lett. **92**, 117407 (2004).

[6] R. Goldhahn, S. Shokovets, V. Cimalla, L. Spiess, G. Ecke, O. Ambacher, J. Furthmüller, F. Bechstedt, H. Lu, and W. J. Schaff, Mater. Res. Soc. Symp. Proc. **743**, L5.9 (2003).

[7] A. Kasic, E. Valcheva, B. Monemar, H. Lu, and W. J. Schaff, Phys. Rev. B **70**, 115217 (2004).

[8] R. Goldhahn, A. T. Winzer, V. Cimalla, O. Ambacher, C. Cobet, W. Richter, N. Esser, J. Furthmüller, F. Bechstedt, H. Lu, and W. J. Schaff, Superlattices Microstruct. **36**, 591 (2004).

[9] A. G. Bhuiyan, A. Hashimoto, and A. Yamamoto, J. Appl. Phys. **94**, 2779 (2003).

[10] A. Zunger, Phys. Rev. B **22**, 5839 (1980).

[11] P. Lawaetz, Phys. Rev. B **5**, 4039 (1972).

[12] A. P. Lima, A. Tabata, J. R. Leite, S. Kaiser, D. Schikora, B. Schöttker, T. Frey, D. J. As, and K. Lischka, J. Cryst. Growth **201/202**, 396 (1999).

[13] V. Cimalla, J. Pezoldt, G. Ecke, R. Kosiba, O. Ambacher, L. Spieß, H. Lu, W. J. Schaff, and G. Teichert, Appl. Phys. Lett. **83**, 3468 (2003).

[14] N. E. Christensen and I. Gorczyca, Phys. Rev. B **50**, 4397 (1994).

[15] L. Bellaiche, K. Kunc, and J. M. Besson, Phys. Rev. B **54**, 8945 (1996).

[16] M. Ueno, M. Yoshida, A. Onodera, O. Shimomura, and K. Takemura, Phys. Rev. B **49**, 14 (1994).

[17] A. F. Wright and J. S. Nelson, Phys. Rev. B **51**, 7866 (1995).

[18] U. Grossner, J. Furthmüller, and F. Bechstedt, Phys. Rev. B **58**, R1722 (1998).

[19] C. Stampfl and C. G. Van de Walle, Phys. Rev. B **59**, 5521 (1999).

[20] F. Bechstedt and J. Furthmüller, J. Cryst. Growth **246**, 315 (2002).

[21] F. Bechstedt, J. Furthmüller, M. Ferhat, L. K. Teles, L. M. R. Scolfaro, J. R. Leite, V. Yu. Davydov, O. Ambacher, and R. Goldhahn, Phys. Status Solidi A **195**, 628 (2003).

[22] D. Bagayoko, L. Franklin, and G. L. Zhao, J. Appl. Phys. **96**, 4297 (2004).

[23] P. Hohenberg and W. Kohn, Phys. Rev. **136**, B864 (1964).

[24] W. Kohn and L. J. Sham, Phys. Rev. **140**, A1133 (1965).

[25] J. P. Perdew and Y. Wang, Phys. Rev. B **33**, R8800 (1986).

[26] J. P. Perdew, in *Electronic Structure of Solids '91*, edited by P. Ziesche and H. Eschrig (Akademie-Verlag, Berlin, 1991), p. 11.

[27] M. S. Hybertsen and S. G. Louie, Phys. Rev. B **34**, 5390 (1986).

[28] F. Bechstedt, Adv. Solid State Phys. **32**, 161 (1992).

[29] A. Rubio, J. L. Corkill, M. L. Cohen, E. L. Shirley, and S. G. Louie, Phys. Rev. B **48**, 11810 (1993).

[30] T. Kotani and M. Schilfgaarde, Solid State Commun. **121**, 461 (2002).
[31] C. Stampfl, C. G. Van de Walle, D. Vogel, P. Krüger, and J. Pollmann, Phys. Rev. B **61**, R7846 (2000).
[32] S. Bei der Kellen and A. J. Freeman, Phys. Rev. B **54**, 11187 (1996).
[33] D. Vogel, P. Krüger, and J. Pollmann, Phys. Rev. B **55**, 12836 (1997).
[34] C. Persson, R. Ahuja, A. Ferreira da Silva, and B. Johansson, J. Phys.: Condens. Matter **13**, 8945 (2001).
[35] A. Sher, M. van Schilfgaarde, M. A. Berding, S. Krishnamurthy, and A-B. Chen, MRS Internet J. Nitride Semicond. Res. **4S1**, G5.1 (1999).
[36] M. Städele, J. A. Majewski, P. Vogl, and A. Görling, Phys. Rev. Lett. **79**, 2089 (1997).
[37] S-H. Wei, X. Nie, I. G. Batyrev, and S. B. Zhang, Phys. Rev. B **67**, 165209 (2003); P. Carrier and S-H. Wei, J. Appl. Phys. **97**, 033707 (2005).
[38] C. P. Foley and T. L. Tansley, Phys. Rev. B **33**, 1430 (1986).
[39] D. Fritsch, H. Schmidt, and M. Grundmann, Phys. Rev. B **67**, 235205 (2003); **69**, 165204 (2004).
[40] F. Bechstedt, J. Furthmüller, O. Ambacher, and R. Goldhahn, Phys. Rev. Lett. **93**, 269701 (2004).
[41] B. Adolph, V. I. Gavrilenko, K. Tenelsen, F. Bechstedt, and R. Del Sole, Phys. Rev. B **53**, 9797 (1996).
[42] T. Schmidtling, M. Drago, U. W. Pohl, and W. Richter, J. Cryst. Growth **248**, 523 (2003).
[43] J. P. Perdew and A. Zunger, Phys. Rev. B **23**, 5048 (1981).
[44] G. Kresse and J. Furthmüller, Comput. Mater. Sci. **6**, 15 (1996); Phys. Rev. B **54**, 11169 (1996).
[45] M. M. Rieger and P. Vogl, Phys. Rev. B **52**, 16567 (1995).
[46] G. Kresse and D. Joubert, Phys. Rev. B **59**, 1758 (1999).
[47] B. Adolph, J. Furthmüller, and F. Bechstedt, Phys. Rev. B **63**, 125108 (2001).
[48] B. Wenzien, G. Cappellini, and F. Bechstedt, Phys. Rev. B **51**, 14701 (1995).
[49] J. Furthmüller, G. Cappellini, H-Ch. Weissker, and F. Bechstedt, Phys. Rev. B **66**, 045110 (2002).
[50] L. J. Sham and T. M. Rice, Phys. Rev. **144**, 708 (1966); W. Hanke and L. J. Sham, Phys. Rev. B **12**, 4501 (1975); **21**, 4656 (1980).
[51] S. Albrecht, L. Reining, R. Del Sole, and G. Onida, Phys. Rev. Lett. **80**, 4510 (1998).
[52] L. X. Benedict, E. L. Shirley, and R. B. Bohn, Phys. Rev. Lett. **80**, 4514 (1998).
[53] M. Rohlfing and S. G. Louie, Phys. Rev. Lett. **83**, 856 (1999).
[54] H. J. Monkhorst and J. D. Pack, Phys. Rev. B **13**, 5188 (1976).
[55] W. G. Schmidt, S. Glutsch, P. H. Hahn, and F. Bechstedt, Phys. Rev. B **67**, 085307 (2003).
[56] P. H. Hahn, W. G. Schmidt, and F. Bechstedt, Phys. Rev. Lett. **88**, 016402 (2002).
[57] P. H. Hahn, W. G. Schmidt, K. Seino, M. Preuss, F. Bechstedt, and J. Bernholc, Phys. Rev. Lett. **94**, 037404 (2005).
[58] F. D. Murnaghan, Proc. Natl. Acad. Sci. U.S.A. **30**, 244 (1944).
[59] C-Y. Yeh, Z. W. Lu, S. Froyen, and A. Zunger, Phys. Rev. B **46**, 10086 (1992).
[60] W. Paszkowicz, R. Cerný, and S. Krukowski, Powder Diffr. **18**, 114 (2003).
[61] R. Juza and H. Hahn, Z. Anorg. Allg. Chem. **239**, 282 (1938).
[62] F. Bechstedt, in *Low-Dimensional Nitride Semiconductors*, edited by B. Gil (Oxford University Press, Oxford, 2002), p. 11.
[63] Q. X. Guo, M. Nishio, H. Ogawa, A. Wakahara, and A. Yoshida, Phys. Rev. B **58**, 15304 (1998).
[64] Y. Bu, L. Ma, and M. C. Liu, J. Vac. Sci. Technol. A **11**, 2931 (1993).
[65] K. A. Rickert, A. B. Ellis, F. J. Himpsel, H. Lu, W. J. Schaff, J. M. Redwing, F. Dwikusuma, and T. F. Kuech, Appl. Phys. Lett. **82**, 3254 (2003).
[66] R. Enderlein and N. J. M. Horing, *Fundamentals of Semiconductor Physics and Devices* (World Scientific, Singapore, 1997).
[67] F. Bechstedt and R. Del Sole, Phys. Rev. B **38**, 7710 (1988).
[68] O. Pulci, F. Bechstedt, G. Onida, R. Del Sole, and L. Reining, Phys. Rev. B **60**, 16758 (1999).
[69] S. H. Wei and A. Zunger, Phys. Rev. B **37**, 8958 (1988).
[70] U. Grossner, J. Furthmüller, and F. Bechstedt, Phys. Status Solidi B **216**, 675 (1999).
[71] M. Rohlfing, P. Krüger, and J. Pollmann, Phys. Rev. B **57**, 6485 (1998).
[72] W. A. Harrison, *Elementary Electronic Structure* (World Scientific, Singapore, 1999).
[73] M. Cardona and N. E. Christensen, Solid State Commun. **116**, 421 (2000).
[74] I. Mahboob, T. D. Veal, L. F. J. Piper, C. F. McConville, H. Lu, W. J. Schaff, J. Furthmüller, and F. Bechstedt, Phys. Rev. B **69**, 201307(R) (2004).
[75] H. Lüth, *Solid Surfaces, Interfaces and Thin Films* (Springer, Berlin, 2001).
[76] J. Tersoff, Phys. Rev. B **32**, R6968 (1985).
[77] W. Mönch, J. Appl. Phys. **80**, 5076 (1996).
[78] W. Mönch, *Electronic Properties of Semiconductor Interfaces* (Springer, Berlin, 2004).
[79] M. R. Phillips, M. H. Zareie, O. Gelhausen, M. Drago, T. Schmidtling, and W. Richter, J. Cryst. Growth **269**, 106 (2004).
[80] J. Wu, W. Walukiewicz, W. Shan, K. M. Yu, J. W. Ager III, E. E. Haller, H. Lu, and W. J. Schaff, Phys. Rev. B **66**, 201403(R) (2002).
[81] T. Inushima, M. Higashiwaki, and T. Matsui, Phys. Rev. B **68**, 235204 (2003).
[82] J. Misek and F. Srobar, Elektrotech. Cas. **30**, 690 (1979).
[83] V. Yu. Davydov, A. A. Klochikhin, V. V. Emtsev, D. A. Kundyukov, S. V. Ivanov, V. A. Vekshin, F. Bechstedt, J. Furthmüller, J. Aderhold, J. Graul, A. V. Mudryi, H. Harima, A. Hashimoto, A. Yamamoto, and E. E. Haller, Phys. Status Solidi B **234**, 787 (2002).
[84] W. Walukiewicz, S. X. Li, J. Wu, K. M. Yu, J. W. Ager III, E. E. Haller, H. Lu, and W. J. Schaff, J. Cryst. Growth **269**, 119 (2004).
[85] T. Kotani (private communication).
[86] H. Ehrenreich and M. H. Cohen, Phys. Rev. **115**, 786 (1959).
[87] P. E. Blöchl, O. Jepsen, and O. K. Andersen, Phys. Rev. B **49**, 16223 (1994).
[88] E. O. Kane, J. Phys. Chem. Solids **1**, 249 (1957).
[89] C. Hamaguchi, *Basic Semiconductor Physics* (Springer, Berlin, 2001).
[90] J. Wu, W. Walukiewicz, S. X. Li, R. Armitage, J. C. Ho, E. R. Weber, E. E. Haller, H. Lu, W. J. Schaff, A. Barcz, and R. Jakiela, Appl. Phys. Lett. **84**, 2805 (2004).